Published in final edited form as:
NMR Biomed. 2008 October ; 21(8): 899–907. doi:10.1002/nbm.1279.

Proton imaging of siloxanes to map tissue oxygenation levels (PISTOL): a tool for quantitative tissue oximetry†

Vikram D. Kodibagkar[1], **Xianghui Wang**[1], **Jesús Pacheco-Torres**[1,2], **Praveen Gulaka**[1], and **Ralph P. Mason**[1,*]

[1]Cancer Imaging Program, Department of Radiology, University of Texas Southwestern Medical Center, Dallas, TX, USA

[2]Instituto de Investigaciones Biomédicas 'Alberto Sols', CSIC, Madrid, Spain

Abstract

Hexamethyldisiloxane (HMDSO) has been identified as a sensitive proton NMR indicator of tissue oxygenation (pO_2) based on spectroscopic spin-lattice relaxometry. A rapid MRI approach has now been designed, implemented, and tested. The technique, proton imaging of siloxanes to map tissue oxygenation levels (PISTOL), utilizes frequency-selective excitation of the HMDSO resonance and chemical-shift selective suppression of residual water signal to effectively eliminate water and fat signals and pulse-burst saturation recovery ^{1}H echo planar imaging to map T_1 of HMDSO and hence pO_2. PISTOL was used here to obtain maps of pO_2 in rat thigh muscle and Dunning prostate R3327 MAT-Lu tumor-implanted rats. Measurements were repeated to assess baseline stability and response to breathing of hyperoxic gas. Each pO_2 map was obtained in 3½ min, facilitating dynamic measurements of response to oxygen intervention. Altering the inhaled gas to oxygen produced a significant increase in mean pO_2 from 55 Torr to 238 Torr in thigh muscle and a smaller, but significant, increase in mean pO_2 from 17 Torr to 78 Torr in MAT-Lu tumors. Thus, PISTOL enabled mapping of tissue pO_2 at multiple locations and dynamic changes in pO_2 in response to intervention. This new method offers a potentially valuable new tool to image pO_2 *in vivo* for any healthy or diseased state by ^{1}H MRI.

Keywords

oximetry; oxygen tension; muscle; prostate tumor; echo planar imaging (EPI); water and fat suppression; hexamethyldisiloxane

INTRODUCTION

There is increasing evidence that hypoxia stimulates angiogenesis and metastasis and that hypoxic tumors are more aggressive (1). Furthermore, extensive hypoxia has been associated with poor clinical prognosis for several tumor types, notably cervical and head and neck, based on electrode measurements (2–4). Extensive hypoxia has also been identified in prostate, breast, and brain tumors (5–7). It is expected from definitive observations in cell culture (8) and preclinical investigations in rats and mice (1,9–11) that hypoxic tumors resist radiotherapy. Measurement of tumor hypoxia is becoming

†Presented in part at the 14th Annual Meeting of the International Society of Magnetic Resonance in Medicine, Seattle, 2006

*Correspondence to: R. P. Mason, Department of Radiology, University of Texas Southwestern Medical Center, 5323 Harry Hines Boulevard, Dallas, TX 75390-9058, USA. ralph.mason@utsouthwestern.edu..

increasingly pertinent, as therapy can now be tailored to the characteristics of individual tumors, i.e. personalized medicine. An adjuvant intervention may be applied to patients with hypoxic tumors, e.g. hyperoxic gas breathing to reduce hypoxic fraction. Alternatively, for tumors that resist modulation, a radiation boost may be applied using intensity modulated radiation therapy, or a hypoxic-cell-selective cytotoxin, such as tirapazamine, may be administered.

The ability to measure tissue oxygen tension (pO_2) non-invasively may be important in understanding the physiology, pathophysiology, and, potentially, clinical prognosis of diseases such as cancer and stroke. To date, many assays have examined hypoxia, rather than pO_2 itself. Radionuclide approaches using fluoromisonidazole and copper diacetyl-bis(N^4-methylthiosemicarbazone) can identify hypoxia and have shown predictive value in clinical studies (1). Likewise, immunohistochemistry of biopsy samples after pimonidazole or EF5 (a fluorinated derivative of etanidazole) administration and trapping in tumor tissues have been correlated with outcome (7,12). MRI is particularly suitable for multiple repeat measurements for observing dynamic changes in tissue oxygenation in response to intervention, and blood-oxygen-level-dependent (BOLD) contrast gives an indication of vascular oxygenation, albeit usually qualitative (13–15). ^{19}F NMR can provide quantitative oximetry based on spin-lattice relaxation of perfluorocarbons (16), although it is currently limited to preclinical studies, as reviewed in detail (17,18). The technique has been used to evaluate the ability to manipulate tumor pO_2 based on hyperoxic gas breathing. Most significantly, correlations have been shown between pO_2 at the time of irradiation and growth delay in Dunning prostate R3327-HI and R3327-AT1 rat tumors (10,11) using hexafluorobenzene (HFB) as a reporter molecule.

Although ^{19}F-MR oximetry is well established and continues to make important contributions to basic research, its clinical translation is hampered by the continuing lack of ^{19}F capability on most clinical MRI scanners. Recently, hexamethyldisiloxane (HMDSO) was identified as a ^{1}H-NMR probe of pO_2, and the feasibility of tissue oximetry was presented using ^{1}H-NMR spectroscopic relaxometry of HMDSO, after direct intra-tissue injection (19). With the use of the spectroscopic approach, localization was achieved by virtue of a discrete injection site. The present study demonstrates the implementation of an imaging-based method: proton imaging of siloxanes to map tissue oxygenation levels (PISTOL). As proof of principle, phantom studies are presented and this pO_2 reporter molecule is used to investigate dynamic changes in pO_2 in rat thigh muscle and syngeneic Dunning prostate R3327-MAT-Lu tumors in response to respiratory challenge with oxygen. A comparative ^{19}F-MR oximetry study was also carried out in rat thigh muscle using HFB.

METHODS

Pulse sequence for measuring pO_2

NMR experiments were performed using a Varian Inova® 4.7 T horizontal-bore system equipped with actively shielded gradients. A chemical-shift selective (CHESS) spin-echo sequence was used to identify the location of HMDSO. A spin-echo echo planar imaging (EPI)-based pulse sequence (Fig. 1) was then used for measuring T_1 values for this slice location. The sequence consisted of an initial pulse-burst saturation recovery (PBSR) preparation sequence with 20 non-selective saturation pulses (inter-pulse delay = 50 ms) followed by a variable delay, t, for magnetization recovery. Three CHESS (20) pulses can be included at the end of τ for optional frequency-selective saturation of water and fat. A spin-echo EPI acquisition, consisting of a frequency-selective $\pi/2$ pulse (on-resonance for HMDSO), a slice-selective π pulse, and an EPI readout, follows τ. A long echo time (~50 ms) was used, which aided suppression of the fat resonance. This combination of PBSR with frequency-selective excitation EPI (HMDSO) and suppression (water, fat) allowed T_1

mapping of HMDSO in 3½ min. For ^{19}F-MR oximetry experiments, FREDOM (fluorocarbon relaxometry using echo planar imaging for dynamic oxygen mapping) was applied using a standard EPI sequence with PBSR (17). The location of HFB was easily determined by using a standard spin-echo sequence, because of the lack of ^{19}F background signal. In both cases (^{1}H and ^{19}F), T_1 values were obtained using the corresponding sequence with the ARDVARC (alternating relaxation delays with variable acquisitions for reduction of clearance effects) protocol (21). Varying τ in the range 0.1–55 s, gave a total acquisition time of 3½ min per T_1 measurement for PISTOL. T_1, R_1 (=1/T_1) and pO_2 maps were computed on a voxel-by-voxel basis using a home-built program written in Matlab (Mathworks Inc., Nattick, MA, USA). For a given voxel, the T_1 value was obtained by a three-parameter least-squares curve fit of the signal intensities corresponding to 16 τ values using the Levenberg–Marquardt algorithm. The R_1 maps were converted into pO_2 maps using previously published calibration curves (19).

Phantom experiments—A phantom consisting of tubes containing water, mineral oil (to simulate fat), and HMDSO was used to optimize the pulse sequence and test water and fat suppression. To measure the pO_2 vs R_1 calibration curve by imaging, a second phantom consisting of four gas-tight John Young NMR tubes (Wilmad Labglass, Buena, NJ, USA) containing 1 mL HMDSO each bubbled with different concentrations of O_2 (0%, 5%, 10%, and 21% calibrated gases; Airgas Southwest, Dallas, TX, USA) was used. Temperature was kept constant with aD_2O-filled circulating water pad and monitored using a fiber-optic temperature probe (FISO Technologies Inc., Quebec City, Quebec, Canada). Mean intensities of each region of interest corresponding to each tube were obtained from the T_1 maps and converted into R_1 values. Measurements were repeated six times to provide mean R_1 values to obtain a calibration curve.

In vivo experiments

The animal investigations were approved by the Institutional Animal Care and Use Committee. Ten healthy Copenhagen-2331 rats (Harlan, Indianapolis, IN, USA) were used to obtain pO_2 data in the thigh muscle (six rats for HMDSO studies and four separate rats for HFB studies). A further six male Copenhagen rats were implanted with Dunning prostate R3327 MAT-Lu tumors subcutaneously on the thigh, to obtain pO_2 data in tumors. Tumors were allowed to grow to a range of sizes from 1.2 to 10.6 cm^3 (five were > $3cm^3$). For MRI, rats were maintained under general gaseous anesthesia (air and 1.5% isoflurane; Baxter International Inc, Deerfield, IL, USA). For pO_2 measurements *in vivo*, 50 μL HMDSO (99.7%; Alfa Aesar, Ward Hill, MA, USA) was administered along two or three tracks in the thigh muscle (n = 6) or MAT-Lu tumors (n = 6) in a single plane using a Hamilton syringe with a 32G needle, as described in detail previously for the analogous ^{19}F-NMR approach (17). For comparative ^{19}F-MR pO_2 measurements, 50 μL HFB (99.9%; Lancaster Co., Pelham, NH, USA) was administered in the thigh muscle, in a separate cohort of animals (n = 4), as above. The rats were placed in the magnet in the prone position, and body temperature was maintained using a warm water blanket. The thigh or tumor was placed inside a size-matched single-turn ^{1}H/^{19}F tunable volume coil. A cross-section through the thigh or tumor was imaged after HMDSO or HFB was located, as described above. In order to modulate tissue oxygenation, the rats were subjected to respiratory challenge in the sequence, air (20 min) – oxygen (30 min) – air (30 min), and T_1 datasets were acquired every 5 min. pO_2 values were obtained from the R_1 values. Typically, 16 pO_2 maps were obtained over a period of 80 min. The statistical significance of changes in pO_2 was assessed by using analysis of variance on the basis of Fisher's protected least-squares difference test at 95% confidence level (Statview, SAS Institute, Carey, NC, USA).

RESULTS

Phantom studies

Suppression of water and mineral oil signals using the spectrally selective spin-echo EPI sequence (Fig. 1) was successful in a water-filled phantom containing smaller tubes of HMDSO and mineral oil (Fig. 2a,b). T_1 measurements from the phantom comprising sealed HMDSO tubes with different oxygen concentrations (at 36.5°C) yielded T_1 values essentially identical with those reported previously by spectroscopy (19) (Fig. 2c,d,e). A linear fit to the data yielded a calibration curve $R_1 = (0.108 \pm 0.001) + (0.00130 \pm 0.00001) \times pO_2$ at 36.5°C.

Tissue oxygenation

HMDSO was readily observed in thigh muscle and tumors by PISTOL with complete suppression of fat and water signals. Discrete distribution of HMDSO was seen in thigh muscle (Fig. 3a,b) and a MAT-Lutumor (Fig. 3f,g) using the CHESS spin-echo sequence. These appear spatially similar to the images of HMDSO and the corresponding pO_2 maps acquired using PISTOL (Fig. 3c–e and 3h–j). The imaging data revealed the pO_2 distribution, showing the effect of breathing oxygen. Baseline pO_2 values were obtained by averaging four baseline pO_2 measurements while the rats breathed air. In rat thigh muscle (n = 6), mean baseline pO_2 ranged from 27 to 71 Torr (mean = 55 ± 17 Torr), but was stable in any given muscle (mean variation = ±4 Torr over 20 min). On alteration of inhaled gas to oxygen, mean pO_2 increased significantly (Fig. 4a) and continued to increase over 20 min. For the group of thigh muscles, mean pO_2 was significantly elevated ($P < 0.05$) compared with baseline by the first measurement (5 min) after the switch of inhaled gas to oxygen and reached values of 163–290 Torr (mean pO_2 = 238 ± 59 Torr) after 30 min of breathing oxygen. On return to air breathing, mean pO_2 had decreased significantly by the first measurement (5 min) and had returned to a value not significantly different from baseline by the second measurement (10 min). Measurements of pO_2 in thigh muscle using HFB yielded similar results (Fig. 4b). For this group (n = 4), mean baseline pO_2 ranged from 23 to 51 Torr (mean = 35 ± 11 Torr), and was stable in any given muscle (mean variation = 3 Torr over 20 min). In response to oxygen breathing, mean pO_2 was significantly elevated ($P < 0.05$) compared with baseline by the first measurement (5 min) after the switch of inhaled gas to oxygen and had reached values of 152–305 Torr (mean pO_2 = 211 ± 79 Torr) after 30 min of breathing oxygen. On return to air breathing, mean pO_2 had decreased significantly by the third measurement (15 min) and had returned to a value not significantly different from baseline by the fourth measurement (20 min).

In rat prostate MAT-Lu tumors (n = 6), mean baseline pO_2 ranged from −0.5 to 41 Torr (mean = 17 ± 16 Torr), but was stable in each tumor (mean variation = ±2 Torr over 20 min). Tumors 1–5 showed a mean baseline pO_2 = 12 ± 12 Torr with a mean variation of ±2 Torr. For these five tumors, mean pO_2 was significantly elevated ($P < 0.05$) compared with baseline by the fifth measurement (25 min) after the switch of inhaled gas to oxygen (Fig. 5). When oxygen was breathed for 30 min, mean pO_2 reached 30 ± 27 Torr (range 7–69). On switching back to air from oxygen, mean pO_2 had returned to a value not significantly different from baseline by the second measurement (10 min). Tumor 6 exhibited particularly high pO_2 response to breathing oxygen (mean pO_2 = 323 ± 44 Torr after 30 min of oxygen breathing), which was very different from the other tumors. Comparing the ^1H anatomical (H_2O) and selective HMDSO images showed that the HMDSO was deposited in the tumor periphery and was probably not representative of the tumor bulk. Hence, it has been excluded from Fig. 5. Figure 6 shows histograms of pO_2 distributions for pooled voxels from rat thigh muscle (Fig. 6a) and MAT-Lu tumors (Fig. 6b) and changes in the distribution after 30 min of oxygen breathing. Figure 7 shows the changes in representative

voxels (five each) from a representative muscle (Fig. 7a) and tumor (Fig. 7b, same tumor as shown in Fig. 3). Data for individual tumors are summarized in Table 1.

DISCUSSION

HMDSO has previously been shown to be a promising ^{1}H-MR-based pO_2 reporter molecule for spectroscopic *in vivo* studies based on the linear dependence of its spin-lattice relaxation rate R_1 on pO_2 at a given temperature in the range 26–46°C (19). The present study demonstrates the feasibility of imaging dynamic changes in tissue oxygenation using frequency-selective EPI of HMDSO, after direct injection into tissue.

In seeking a proton NMR pO_2 reporter molecule, HMDSO was selected for its similarity to traditional ^{19}F-NMR perfluorocarbon agents. HMDSO is hydrophobic and is essentially immiscible with aqueous solutions. Thus, gas exchange with the surrounding tissue occurs without exchange of ions, which might influence the spin lattice relaxation; thus, the validity of *in vitro* calibrations is maintained for *in vivo* determinations. HMDSO is readily available, inexpensive, and easy to store. Although HMDSO was used here, other symmetric, hydrophobic siloxanes may also be effective pO_2 reporter molecules, and this new concept is open to development and optimization. In the perfluorocarbon field, many different molecules have been exploited for *in vivo* oximetry over the years (22,23). Initially, perfluorocarbon blood substitute emulsions were favored for their biocompatibility, but multi-resonance molecules, such as perfluorotributylamine and perflubron (perfluoro-octylbromide) were suboptimal for oximetry, because of relatively low R_1 dependence on pO_2 and high dependence on temperature (22). Moreover, the multi-resonance spectra caused considerable signal loss for imaging (24). Ultimately, HFB and perfluoro-15-crown-5 ether were identified as superior because of their single resonances (18,25,26), and HFB is particularly attractive because of its low temperature dependence and ready commercial availability. Just as the perfluorocarbon oximetry field has evolved, other siloxanes may be identified or developed that may be superior to HMDSO.

Mapping pO_2 was demonstrated using frequency-selective excitation of the HMDSO resonance with efficient frequency-selective fat and water suppression *in vitro* and *in vivo*. The calibration curve obtained here with imaging compares well with the calibration curve obtained previously by spectroscopy (19). Clearance of HMDSO from tissues (half-life ~35 h) is relatively slow compared with clearance of HFB used in the analogous ^{19}F-MR oximetry (FREDOM) (17,27), so that there is minimal clearance during a typical investigation of oxygen dynamics in response to acute interventions (19). Thus, although FREDOM provides sensitive assessment of acute changes in response to respiratory challenge or vascular targeting agents, the slower clearance of HMDSO may facilitate studies of chronic changes in tumor oxygenation accompanying tumor growth or long-term chemotherapy. Application of HMDSO to breast studies could be difficult in the presence of silicone implants because of the similar chemical shifts.

In rat thigh muscle, the range of baseline pO_2 values measured by PISTOL and pO_2 response to oxygen challenge were similar to those measured here by the well-established ^{19}F-MR oximetry technique and those reported previously using ^{1}H spectroscopy of HMDSO (19) or ^{19}F MRI of HFB (28), needle electrodes, fiber optical probes (29,30), or electron paramagnetic resonance (31,32). The response of individual voxels and muscles in separate rats to oxygen breathing depends on voxel location (Figs. 3,4,6, and 7), but the baseline values and response are generally higher than seen in tumors. As also reported by Yeh *et al.* (33), based on measurements using oxygen electrodes, the pO_2 of Dunning prostate tumors tends to be lower than in skeletal muscle. The baseline pO_2 values and pO_2 response to oxygen challenge are quite similar to those reported previously

for large MAT-Lu tumors using ^{19}F-MR oximetry (34). Different rat prostate and breast tumor types are reported to exhibit a range of baseline oxygenations, and the response to interventions is highly variable. In some cases, hypoxic fractions resist modulation with hyperoxic gas breathing [e.g. Dunning prostate R3327-AT1 tumors (10,35)]. In other tumors, notably with a well-developed and highly perfused vasculature, hyperoxic gas essentially eliminated hypoxia [large Dunning prostate R3327-HI tumors (11)].

Direct intratumoral injection of the reporter molecule has benefits and drawbacks. It allows immediate measurement of any region of interest after minimally invasive administration. By contrast, reporter molecules administered systemically initially report vascular oxygenation (36) and even after clearance tend to sequester in well-perfused regions biasing measurements (37). Of course, direct injection does limit measurements to accessible tissues. It would be preferable to exploit endogenous molecules as used in BOLD contrast, but this reveals vascular oxygenation and is subject to variations in vascular volume, hematocrit, and flow (13,14). Direct measurements of tissue water T_1 are attractive (38,39), but they may be influenced by many factors in addition to pO_2. Like perfluorocarbons, HMDSO is lipophilic and is essentially immiscible in aqueous solutions. It could be emulsified for systemic delivery to help circumvent the need for direct intra-tissue injections, and such an attempt is currently underway. Some silanes are highly reactive, whereas HMDSO is quite inert, and is reported to exhibit minimal toxicity (40,41). In a 13-week subchronic inhalation toxicity study in Fischer 344 rats exposed to 5000 ppm of HMDSO, no treatment-related signs of toxicity or mortality, or other significant histological changes were found (40). After oral (300 mg/kg) or intravenous administration (80 mg/kg, as emulsion) of HMDSO, various polar metabolites were found in the urine as a result of the oxidation of the $Si–CH_3$ bond (42). Another study reported no irritation in Draize tests of skin or eye irritancy and no acute toxicity in rats (LD_{50} > 3.8 g/kg) (43). In our studies, we saw no overt signs of inflammation or discomfort, although no microscopic analyses were performed. For future routine use as an intra-tissue-injected pO_2 reporter molecule, further investigation of possible local inflammatory response after direct injection of siloxanes is warranted.

In summary, PISTOL is a sensitive, quantitative ^{1}H-MR method for imaging oxygen tension and dynamic changes in response to interventions. This new technique opens up further opportunities to evaluate pO_2 *in vivo*. Rapid translation of this method to the clinical setting is feasible with current state-of-the-art MR hardware, as clinical instruments can routinely generate effective water and fat suppression as used in detection of metabolites such as choline, lactate, and citrate. A further advantage of PISTOL is that it will now be possible to add quantitative oximetry to a protocol consisting of other ^{1}H-MR-based functional techniques routinely used for research as well as clinical diagnosis, such as dynamic contrast enhancement, diffusion measurements, and MRS.

Acknowledgments

We are grateful to Jennifer McAnally for assistance in tumor implantation and to Drs Dawen Zhao, Weina Cui, and Mark Conradi for constructive suggestions. We appreciate the help of Glenn Katz in preparing the figures. We also thank Dr Maj Hedehus (Varian Inc., Palo Alto, CA, USA) for helpful tips in pulse sequence programming. J.P.T. gratefully acknowledges a fellowship from the Communidad de Madrid. This work was supported in part by the DOD Prostate Cancer Initiative (W81XWH-06-1-0149). The MR investigations were performed at the Advanced Imaging Research Center, an NIH BRTP facility (P41RR02584) in conjunction with the Small Animal Imaging Research Program (NCI U24 CA126608).

Contract/grant sponsor: DAMD; *contract/grant number:* W81XWH-06-1-0149.

Contract/grant sponsor: NIH; *contract/grant number:* P41RR02584.

Contract/grant sponsor: NIH; *contract/grant number:* U24 CA126608.

Abbreviations used

ARDVARC	alternating relaxation delays with variable acquisitions for reduction of clearance effects data acquisition protocol
BOLD	blood oxygen level dependent
CHESS	chemical-shift selective
EPI	echo planar imaging
FREDOM	fluorocarbon relaxometry using echo planar imaging for dynamic oxygen mapping
HFB	hexafluorobenzene
HMDSO	hexamethyldisiloxane
MAT-Lu	Dunning prostate R3327-AT tumor subline metastatic to lungs
PBSR	pulse-burst saturation recovery
pO_2	oxygen tension
PISTOL	proton imaging of siloxanes to map tissue oxygenation levels

REFERENCES

1. Tatum JL, Kelloff GJ, Gillies RJ, Arbeit JM, Brown JM, Chao KS, Chapman JD, Eckelman WC, Fyles AW, Giaccia AJ, Hill RP, Koch CJ, Krishna MC, Krohn KA, Lewis JS, Mason RP, Melillo G, Padhani AR, Powis G, Rajendran JG, Reba R, Robinson SP, Semenza GL, Swartz HM, Vaupel P, Yang D, Croft B, Hoffman J, Liu G, Stone H, Sullivan D. Hypoxia: importance in tumor biology, noninvasive measurement by imaging, and value of its measurement in the management of cancer therapy. Int. J. Radiat. Biol 2006;82:699–757. [PubMed: 17118889]
2. Fyles A, Milosevic M, Hedley D, Pintilie M, Levin W, Manchul L, Hill RP. Tumor hypoxia has independent predictor impact only in patients with node-negative cervix cancer. J. Clin. Oncol 2002;20:680–687. [PubMed: 11821448]
3. Fyles A, Milosevic M, Pintilie M, Syed A, Levin W, Manchul L, Hill RP. Long-term performance of interstial fluid pressure and hypoxia as prognostic factors in cervix cancer. Radiother. Oncol 2006;80:132–137. [PubMed: 16920212]
4. Brizel DM, Sibly GS, Prosmitz LR, Scher RL, Dewhirst MW. Tumor hypoxia adversely affects the prognosis of carcinoma of the head and neck. Int. J. Radiat. Oncol. Biol. Phys 1997;38:285–289. [PubMed: 9226314]
5. Movsas B, Chapman JD, Hanlon AL, Horwitz EM, Greenberg RE, Stobbe C, Hanks GE, Pollack A. Hypoxic prostate/muscle pO_2 ratio predicts for biochemical failure in patients with prostate cancer: preliminary findings. Urology 2002;60:634–639. [PubMed: 12385924]
6. Vaupel PW, Schlenger K, Knoop C, Höckel M. Oxygenation of human tumors: evaluation of tissue oxygen distribution in breast cancers by computerized O_2 tension measurements. Cancer Res 1991;51:3316–3322. [PubMed: 2040005]
7. Evans SM, Judy KD, Dunphy I, Jenkins WT, Nelson PT, Collins R, Wileyto EP, Jenkins K, Hahn SM, Stevens CW, Judkins AR, Phillips P, Geoerger B, Koch CJ. Comparative measurements of hypoxia in human brain tumors using needle electrodes and EF5 binding. Cancer Res 2004;64:1886–1892. [PubMed: 14996753]
8. Gray L, Conger A, Ebert M, Hornsey S, Scott O. The concentration of oxygen dissolved in tissues at time of irradiation as a factor in radiotherapy. Br. J. Radiol 1953;26:638–648. [PubMed: 13106296]
9. O'Hara JA, Goda F, Demidenko E, Swartz HM. Effect on regrowth delay in a murine tumor of scheduling split-dose irradiation based on direct pO_2 measurements by electron paramagnetic resonance oximetry. Radiat. Res 1998;150:549–556. [PubMed: 9806597]

10. Bourke VA, Zhao D, Gilio J, Chang C-H, Jiang L, Hahn EW, Mason RP. Correlation of radiation response with tumor oxygenation in the Dunning prostate R3327-AT1 tumor. Int. J. Radiat. Oncol. Biol. Phys 2007;67:1179–1186. [PubMed: 17336219]
11. Zhao D, Constantinescu A, Chang C-H, Hahn EW, Mason RP. Correlation of tumor oxygen dynamics with radiation response of the Dunning prostate R3327-HI tumor. Radiat. Res 2003;159:621–631. [PubMed: 12710873]
12. Kaanders JHAM, Wijffels KIEM, Marres HAM, Ljungkvist ASE, Pop LAM, van den Hoogen FJA, de Wilde PCM, Bussink J, Raleigh JA, van der Kogel AJ. Pimonidazole binding and tumor vascularity predict for treatment outcome in head and neck cancer. Cancer Res 2002;62:7066–7074. [PubMed: 12460928]
13. Howe FA, Robinson SP, McIntyre DJ, Stubbs M, Griffiths JR. Issues in flow and oxygenation dependent contrast (FLOOD) imaging of tumours. NMR Biomed 2001;14:497–506. [PubMed: 11746943]
14. Baudelet C, Gallez B. Current issues in the utility of blood oxygen level dependent MRI for the assessment of modulations in tumor oxygenation. Current Medical Imaging Reviews 2005;1:229–243.
15. Dunn JF, O'Hara JA, Zaim-Wadghiri Y, Lei H, Meyerand ME, Grinberg OY, Hou H, Hoopes PJ, Demidenko E, Swartz HM. Changes in oxygenation of intracranial tumors with carbogen: a BOLD MRI and EPR oximetry study. J. Magn Reson Imaging 2002;16:511–521. [PubMed: 12412027]
16. Kodibagkar VD, Wang X, Mason RP. Physical principles of quantitative nuclear magnetic resonance oximetry. Front Biosci 2008;13:1371–1384. [PubMed: 17981636]
17. Zhao D, Jiang L, Mason RP. Measuring changes in tumor oxygenation. Methods Enzymol 2004;386:378–418. [PubMed: 15120262]
18. Robinson SP, Griffiths JR. Current issues in the utility of ^{19}F nuclear magnetic resonance methodologies for the asssessment of tumour hypoxia. Philos. Trans. R. Soc. London B Biol. Sci 2004;359:987–996. [PubMed: 15306411]
19. Kodibagkar VD, Cui W, Merritt ME, Mason RP. A novel ^{1}H NMR approach to quantitative tissue oximetry using hexamethyldisiloxane. Magn. Reson. Med 2006;55:743–748. [PubMed: 16506157]
20. Haase A, Frahm J, Hanicke W, Matthaei D. H-1-Nmr chemical-shift selective (Chess) imaging. Phys. Med. Biol 1985;30:341–344. [PubMed: 4001160]
21. Hunjan S, Zhao D, Constantinescu A, Hahn EW, Antich PP, Mason RP. Tumor Oximetry: demonstration of an enhanced dynamic mapping procedure using fluorine-19 echo planar magnetic resonance imaging in the Dunning prostate R3327-AT1 rat tumor. Int. J. Radiat. Oncol. Biol. Phys 2001;49:1097–1108. [PubMed: 11240252]
22. Yu JX, Kodibagkar V, Cui W, Mason RP. ^{19}F: a versatile reporter for non-invasive physiology and pharmacology using magnetic resonance. Curr. Med. Chem 2005;12:818–848.
23. Mason RP. Non-invasive physiology: ^{19}F NMR of perfluorocarbon. Artif. Cells Blood Substit Immobil Biotechnol 1994;22:1141–1153. [PubMed: 7849916]
24. Barker BR, Mason RP, Bansal N, Peshock RM. Oxygen tension mapping by ^{19}F echo planar NMR imaging of sequestered perfluorocarbon. J. Magn Reson Imaging 1994;4:595–602. [PubMed: 7949687]
25. Mason RP, Rodbumrung W, Antich PP. Hexafluorobenzene: a sensitive ^{19}F NMR indicator of tumor oxygenation. NMR Biomed 1996;9:125–134. [PubMed: 8892399]
26. Dardzinski BJ, Sotak CH. Rapid tissue oxygen tension mapping using ^{19}F inversion-recovery echo-planar imaging of perfluoro-15-crown-5-ether. Magn. Reson. Med 1994;32:88–97. [PubMed: 8084241]
27. Hunjan S, Mason RP, Constantinescu A, Peschke P, Hahn EW, Antich PP. Regional tumor oximetry: ^{19}F NMR spectroscopy of hexafluorobenzene. Int. J. Radiat. Oncol. Biol. Phys 1998;40:161–171. [PubMed: 9588931]
28. Yu, J-X.; Cui, W.; Zhao, D.; Mason, RP. Non-invasive physiology and pharmacology using ^{19}F magnetic resonance.. In: Tressaud, A.; Haufe, G., editors. Fluorine and Health. Elsevier B.V.; Amsterdam: 2008. p. 198-276.

29. Seiyama, A.; Shiga, T.; Maeda, N. Temperature effect on oxygenation and metabolism of perfused rat hindlimb muscle.. In: Piiper, J.; Goldstick, TK.; Meyer, M., editors. Oxygen Transport to Tissue XII. Plenum Press; New York: 1990. p. 541-547.
30. McKinley BA, Butler BD. Comparison of skeletal muscle P-O_2, P-CO_2, and pH with gastric tonometric P-CO_2 and pH in hemorrhagic shock. Crit Care Mede 1999;27:1869–1877.
31. Vahidi N, Clarkson RB, Liu KJ, Norby SW, Wu M, Swartz HM. In Vivo and in vitro EPR oximetry with fusinite: a new coal-derived, particulate EPR probe. Magn. Res. Med 1994;31:139–146.
32. Sostaric JZ, Pandian RP, Bratasz A, Kuppusamy P. Encapsulation of a highly sensitive EPR active oxygen probe into sonochemically prepared microspheres. J. Phys. Chem. B 2007;111:3298–3303. [PubMed: 17388464]
33. Yeh KA, Biade S, Lanciano RM, Brown DQ, Fenning MC, Babb JS, Hanks GE, Chapman JD. Polarographic needle electrode measurements of oxygen in rat prostate carcinomas: accuracy and reproducibility. Int. J. Radiat. Oncol. Biol. Phys 1995;33:111–118. [PubMed: 7642408]
34. Zhao D, Constantinescu C, Hahn EW, Mason RP. Differential oxygen dynamics in two diverse Dunning prostate R3327 rat tumor sublines (MAT-Lu and HI) with respect to growth and respiratory challenge. Int. J. Radiat. Oncol. Biol. Phys 2002;53:744–756. [PubMed: 12062621]
35. Zhao D, Ran S, Constantinescu A, Hahn EW, Mason RP. Tumor oxygen dynamics: correlation of in vivo MRI with histological findings. Neoplasia 2003;5:308–318. [PubMed: 14511402]
36. Eidelberg D, Johnson G, Barnes D, Tofts PS, Delpy D, Plummer D, McDonald WI. ^{19}F NMR imaging of blood oxygenation in the brain. Magn. Reson. Med 1988;6:344–352. [PubMed: 3362067]
37. Mason RP, Antich PP, Babcock EE, Constantinescu A, Peschke P, Hahn EW. Non-invasive determination of tumor oxygen tension and local variation with growth. Int. J. Radiat. Oncol. Biol. Phys 1994;29:95–103. [PubMed: 8175452]
38. Matsumoto K, Bernardo M, Subramanian S, Choyke P, Mitchell JB, Krishna MC, Lizak MJ. MR assessment of changes of tumor in response to hyperbaric oxygen treatment. Magn. Reson. Med 2006;56:240–246. [PubMed: 16795082]
39. Zaharchuk G, Busse RF, Rosenthal G, Manley GT, Glenn OA, Dillon WP. Noninvasive oxygen partial pressure measurement of human body fluids in vivo using magnetic resonance imaging. Acad Radiol 2006;13:1016–1024. [PubMed: 16843855]
40. Cassidy SL, Dotti A, Kolesar GB, Dochterman LW, Meeks RG, Chevalier HJ. Hexamethyldisiloxane: a 13-week subchronic whole-body vapor inhalation toxicity study in Fischer 344 rats. Int. J. Toxicol 2001;20:391–399. [PubMed: 11797821]
41. Dobrev ID, Reddy MB, Plotzke KP, Varaprath S, McNett DA, Durham J, Andersen ME. Closed-chamber inhalation pharmaco-kinetic studies with hexamethyldisiloxane in the rat. Inhal. Toxicol 2003;15:589–617. [PubMed: 12692732]
42. Varaprath S, McMahon JM, Plotzke KP. Metabolites of hexamethyldisiloxane and decamethylcyclopentasiloxane in Fischer 344 rat urine: a comparison of a linear and a cyclic siloxane. Drug Metab Dispos 2003;31:206–214. [PubMed: 12527702]
43. Parent RA. Acute toxicity data submissions. Int. J. Toxicol 2000;19:331–373.

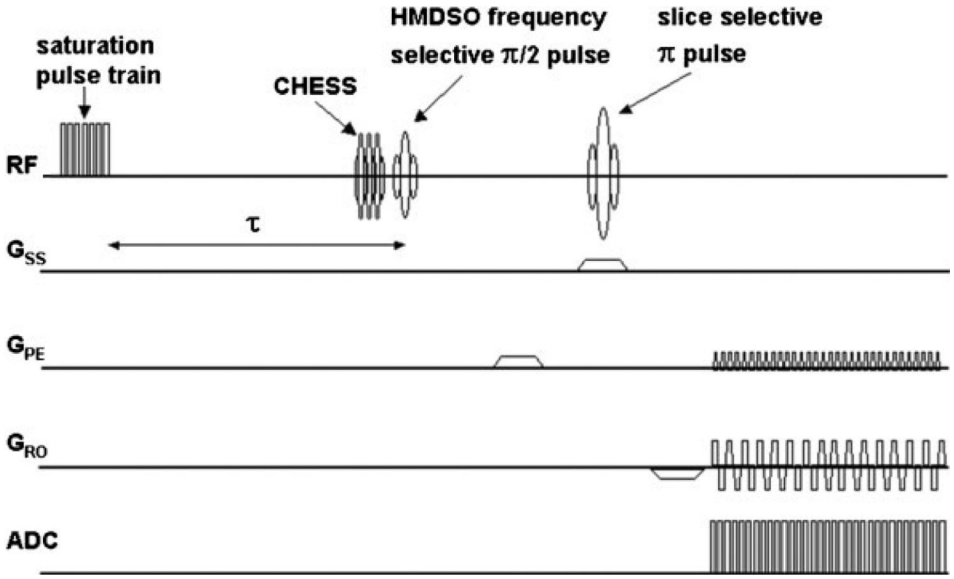

Figure 1.
Pulse sequence for HMDSO relaxometry with optional CHESS fat and water suppression (PISTOL). Magnetization preparation consists of 20 $\pi/2$ saturation pulses followed by a variable recovery time τ. The $\pi/2$ pulse is frequency selective for the HMDSO resonance, whereas the π pulse is slice selective. EPI readout enables T_1 mapping in 3½ min.

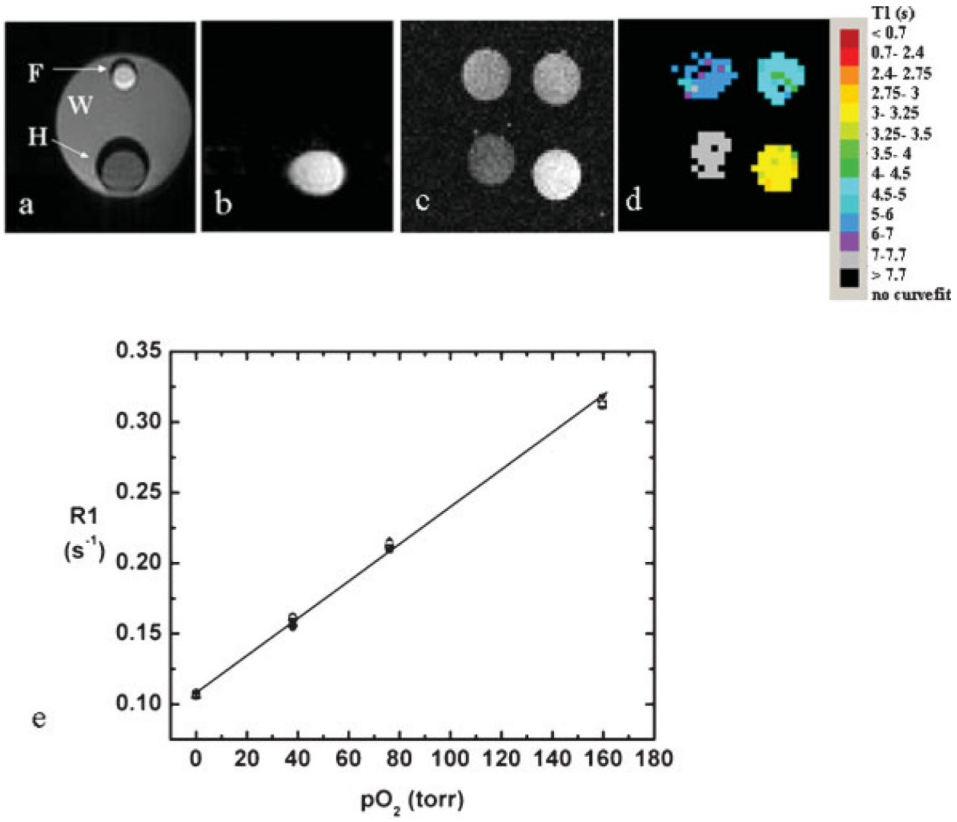

Figure 2.

Water and fat suppression. (a) T_1-weighted spin-echo image of phantom with smaller tubes containing mineral oil (F) and HMDSO (H) inside a tube containing water (W), and (b) EPI image of the same phantom with fat and water suppression. (c) T_1-weighted spin-echo image and (d) T_1 maps of a phantom comprising HMDSO saturated with gases at different concentrations of oxygen (clockwise from bottom left: 0%, 5%, 10% and 21%) obtained using PISTOL. (e) A linear fit to the data (mean region of interest intensities, six measurements) yields the calibration curve: $R_1 = (0.108 \pm 0.001) + (0.00130\ 0.001) \times pO_2$ at 36.5°C.

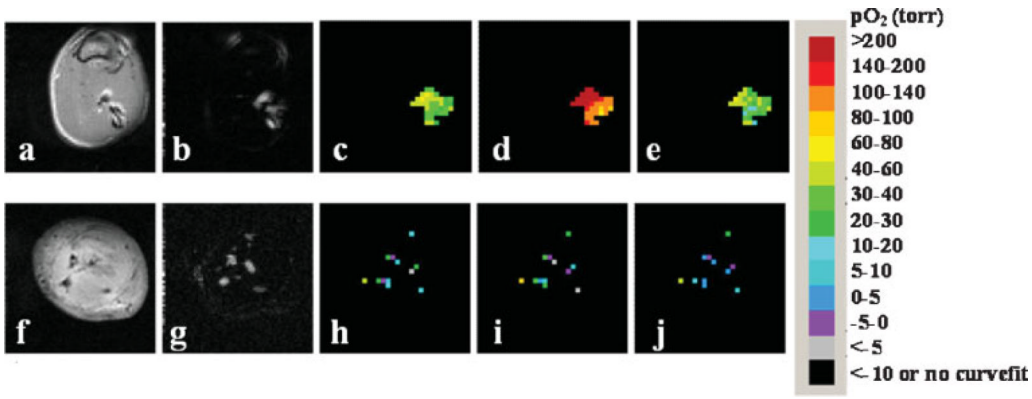

Figure 3.

Monitoring changes in oxygenation of rat thigh muscle and Dunning prostate R3327 prostate MAT-Lu tumors implanted in Copenhagen rat thigh *in vivo* with respect to oxygen challenge. Spin-echo images of a representative rat thigh muscle (a) and MAT-Lu tumor (f). CHESS spin-echo images of silane injected into thigh muscle (b) and tumor (g) showing the distribution of the injected HMDSO. The corresponding time course PISTOL pO_2 maps (c, h, baseline air breathing; d, i, 30 min oxygen; e, j, 30 min after return to air breathing) showing the response to hyperoxic gas intervention in each case.

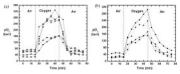

Figure 4.
Dynamic changes in tissue oxygenation measured *in vivo* in rat thigh muscle. Individual curves are shown for mean pO_2 values using (a) HMDSO (n = 6) and (b) HFB (n = 4).

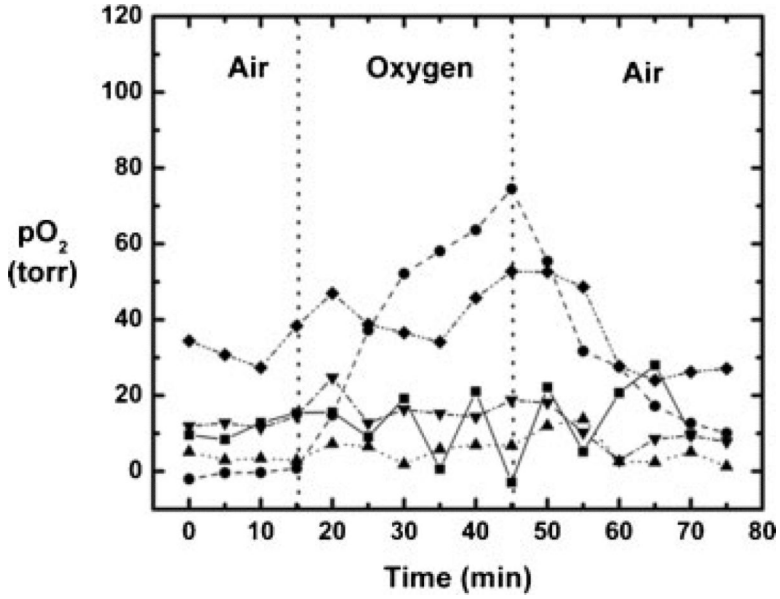

Figure 5.
Dynamic changes in mean tissue oxygenation measured *in vivo* in MAT-Lu tumors (five out of total six) with respect to oxygen challenge. Tumor 6 showed HMDSO only in the tumor periphery and displayed uncharacteristically large response to oxygen challenge. It was excluded from the figure for better visualization of the rest of the data.

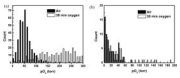

Figure 6.
Distribution of tissue oxygenation measured *in vivo* by PISTOL. Histograms of pO_2 distributions for pooled voxels from (a) rat thigh muscle (n = 6) and (b) MAT-Lu tumors (n = 6) with respect to oxygen challenge.

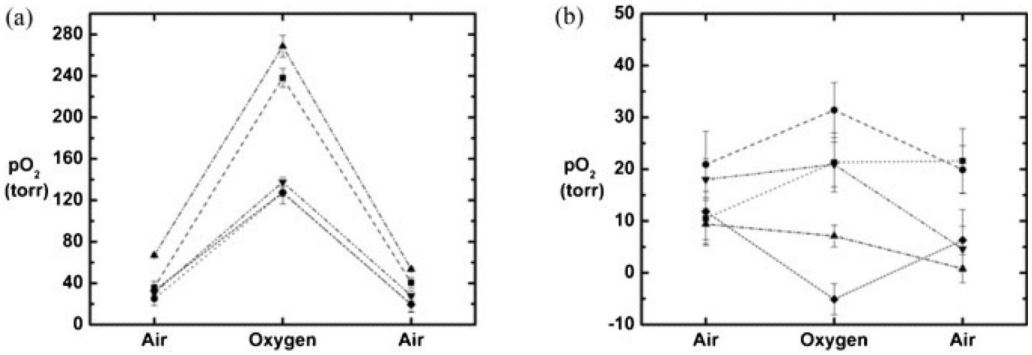

Figure 7.

Dynamic changes in pO_2 values of representative voxels from (a) thigh muscle and (b) rat prostate MAT-Lu tumor. Five voxels were selected from each tissue in Fig. 3 and examined with respect to oxygen challenge. The values are shown during air breathing, 30 min after switching to oxygen, and 30 min after switching back to air. Error bars represent the standard error of curve fit.

Table 1

Mean + SD pO_2 and hypoxic fraction (HF_5, percentage voxels with pO_2 < 5 Torr) for individual tumors with respect to hyperoxic gas challenge in the sequence: air–oxygen–air

	Intervention					
	Air (baseline)		Oxygen		Air (return)	
Tumor number and size (cm^3)	pO_2 (Torr)	HF_5 (%)	pO_2 (Torr)	HF_5 (%)	pO_2 (Torr)	HF_5 (%)
1 (1.2)	11.5 ± 3.2	50	9.1 ± 16.9	72	9.8 ± 11.2	33
2 (10.3)	–0.5 ± 1.2	70	69 ± 7.6*	2**	11.4 ± 1.8*	42**
3 (10.8)	3.6 ± 1.0	71	6.9 ± 0.1*	45*	3.2 ± 2.7	58
4 (3.7)	12.7 ± 1.4	38	16.6 ± 3.2	54	8.6 ± 1.1	57
5 (9.1)	32.7 ± 4.7	56	49.2 ± 4.9**	60	26.6 ± 0.6	58
6[a] (5.6)	40.5 ± 2.7	0	318 ± 6**	0	39.7 ± 2.0	0
Mean ± SD (n = 6)	17 ± 16	48 ± 26	78 ± 120*	39 ± 31	17 ± 14*	41 ± 23
Mean ± SD (n = 5, Nos 1–5)	12 ± 12	57 ± 14	30 ± 27**	47 ± 27	12 ± 19*	50 ± 12

For individual tumors, mean pO_2 or HF_5 was compared between baseline air breathing and the last two measurements with oxygen breathing or return to air.

*$P < 0.05$.

**$P < 0.01$.

[a]Tumor 6 showed unusually high pO_2 and response, and comparison of the ^1H anatomical (H_2O) and selective HMDSO MR images showed that HMDSO had been deposited in the tumor periphery.